High-frequency dynamics of vitreous $GeSe_2$

L. Orsingher*
Physics Department, Trento University, 38050 Povo, Trento, Italy

G. Baldi
European Synchrotron Radiation Facility, BP 220, 38043 Grenoble, France and IPCF-CNR, UOS di Roma, 00185 Roma, Italy

A. Fontana
Physics Department, Trento University, 38050 Povo, Trento, Italy and IPCF-CNR, UOS di Roma, 00185 Roma, Italy

L. E. Bove
DPMD-IMPMC, UMR 7590, Université Pierre et Marie Curie (UPMC), 140, F-75015 Paris, France

T. Unruh
Forschungsneutronenquelle Heinz-Maier-Leibnitz (FRM II), Technische Universität München, 85747 Garching, Germany

A. Orecchini, C. Petrillo, N. Violini, and F. Sacchetti
Physics Department, Perugia University, 06100 Perugia, Italy

(Received 31 March 2010; revised manuscript received 10 June 2010; published 2 September 2010)

The vibrational dynamics of vitreous germanium diselenide (v-$GeSe_2$), an amorphous glass belonging to the family of continuous random network forming glasses, has been investigated by means of inelastic neutron scattering. We employed three different neutron spectrometers, each of them providing different energy resolutions and spanning different portions of the energy-wave-vector $(\hbar\omega, Q)$ plane, which partially overlap so that complementary information can be obtained. Two well-defined peaks are resolved in the dynamic structure factor in a broad Q region, below and above the position of the first sharp diffraction peak in the static structure factor. The low-lying excitation is nondispersive and located around the boson peak frequency. The high-frequency mode presents a pseudoperiodic behavior and it can be associated to the high-frequency counterpart of the longitudinal acoustic (LA) mode. In the low-Q region this mode shows a positive dispersion of its apparent sound velocity and an attenuation which follows a Q^2 law. The combined use of a set of appropriate instruments allows an accurate determination of the nonergodicity parameter $f(Q)$. The LA dispersion curve of v-$GeSe_2$ is similar to that measured in other glasses where a second excitation appears in the spectra. On the contrary other glass forming materials, where this second mode is not detected, present a sinusoidal-like dispersion curve with a deeper minimum in the second pseudo-Brillouin zone.

DOI: 10.1103/PhysRevB.82.115201 PACS number(s): 61.05.fg, 61.43.−j, 63.50.Lm

I. INTRODUCTION

Because of the absence of periodicity, which characterizes the class of amorphous materials, the vibrational eigenstates of the Hamiltonian cannot be easily computed on the basis of translational symmetry tools. In the long wavelength limit, at megahertz frequencies, glasses behave as continuous media and sustain the propagation of sound waves, like their crystal counterparts. Decreasing the wavelength, the vibrational states progressively lose their plane-wave character and the relationship between wave vector Q and energy $\hbar\omega$ is not one to one any more. The main effect of the disorder is the broadening of the spectral distribution of these modes so that they appear as strongly damped in the dynamic structure factor.

The existence of phononlike excitations at high frequency has stimulated both theoretical and experimental efforts[1–8] but a general consensus on the nature of the excitations is still lacking and the understanding of their features is far from the level of knowledge reached in crystals. On the experimental side, the nature of the acousticlike excitations at terahertz (THz) frequencies has been investigated in a number of amorphous materials by means of both inelastic x-ray (IXS) and inelastic neutron scattering (INS). However the majority of these studies has been performed in a limited wave-vector range. The entire dispersion curve has been measured only in a few glasses, such as v-SiO_2,[9–11] v-GeO_2,[12] Se,[13] and ethanol.[14] These studies have revealed the existence in glasses of pseudo-Brillouin zones (BZ), whose boundary is located around one half of the position of the first sharp diffraction peak (FSDP) in the static structure factor. The comparison of the dispersion curve of the longitudinal acoustic (LA) mode of v-$GeSe_2$ with the available literature data for other systems reveals an unexpected difference between strong glasses and fragile glassy ethanol. The dispersion curve maintains a pseudoperiodic behavior which mimics the crystalline case in the ethanol glass, whereas in strong glasses the branch flattens above the first pseudo-BZ boundary, as also confirmed by numerical simulations.[9,12,15] This behavior might suggest a connection between the trend of the dispersion curve and the fragility,[16] which, however, is not observed in the case of fragile lithium diborate glass.[17] Therefore the shape of the dispersion curve

could be related also to the bonding topology of the system, e.g., network versus non-network glasses.[18]

In order to understand how structural disorder influences the properties of the acoustic branches we carried out a detailed study of the high-frequency dynamics in v-$GeSe_2$. Vitreous germanium diselenide is a strong glass with the same structural units of v-SiO_2 and v-GeO_2 but with different intertetrahedral connections and a higher degree of fragility ($m=32$).[19] Various structural studies[20–25] describe a continuous random network of $Ge(Se_{1/2})_4$ tetrahedra with the fourfold coordinated atom at the center and the presence of both edge-sharing and corner-sharing configurations. The diffraction pattern, measured by neutron scattering, shows a FSDP located at a wave-vector transfer $Q_P \approx 1$ Å^{-1}.

The longitudinal sound velocity measured with Brillouin light scattering (BLS) is small enough [2200 m/s (Ref. 26)] for a direct inspection of the vibrational dynamics by means of INS. The present experimental investigation is performed employing three instruments, each of them providing different energy resolutions and spanning different $(Q,\hbar\omega)$ space regions, which partially overlap. The obtained complementary information allow us to resolve two excitations in the dynamic structure factor and to follow the evolution of these modes in a broad Q region, below and above the first sharp diffraction peak.

The low-frequency component is nondispersive and is located around the boson peak frequency. The dispersion curve of the high-frequency mode presents a pseudoperiodic behavior with a pseudo-BZ boundary around $Q=Q_P/2$. In the low-Q range, the dispersion curve extrapolates to a linear dependence corresponding to the longitudinal macroscopic sound velocity. This indicates that the high-frequency component appearing in the dynamic structure factor is the high-frequency evolution of the LA mode. The generalized sound velocity of this excitation increases, in the first-Brillouin zone, above its macroscopic value. Moreover, the investigation of the vibrational dynamics with the aid of three different neutron spectrometers allows us to extract detailed information on the relative intensity of both the elastic and the inelastic peaks and to obtain a reliable estimate of the nonergodicity parameter. Exploiting the wide wave-vector-explored range, we determine the density of vibrational states, which shows a boson peak excess located at the same energy of the low-frequency mode.

The paper is organized as follows. Section II describes the experimental details, including the sample preparation and the INS instrument setups. A discussion of the characteristics and the performances of every neutron spectrometer is presented together with the description of the raw-data correction. Section III is devoted to the analysis of the experimental spectra. In Sec. IV the fitted spectra and the results are presented. The conclusions arising from this experimental investigation are presented in the final section.

II. EXPERIMENT

A. Sample

Vitreous germanium diselenide was prepared by means of the standard melt-quenching method. The starting materials were high purity powders of germanium and selenium from Sigma-Aldrich chemicals. Stoichiometric quantities of the reactants were loaded in quartz tubes, which were evacuated and filled with inert nitrogen gas several times in order to avoid the oxygen contamination of the melt. Finally the tubes were filled with nitrogen at a pressure of 0.2 torr and sealed off.[27] The tubes were heated gradually in a furnace up to 1320 K for 6 h and then kept at this temperature for other 10 h. During this time, the tubes were shaken in order to guarantee the homogeneity of the melt and the complete mixing of the reactants. The furnace temperature was decreased to 1070 K and the tubes were extracted and then rapidly quenched in a water and ice mixture. The amorphous state of the obtained samples was checked with x-ray diffraction.

Concerning the neutron-scattering experiments, we observe that the scattering cross section of $GeSe_2$ is dominated by the coherent contribution since the incoherent scattering cross section of Ge and Se amounts, respectively, to about 2% and 4% of the total.[28,29] This allows a safe inspection of the collective modes in the coherent contribution to the differential scattering cross section with a minimum disturbance from the incoherent scattering processes.

B. INS experiments

In neutron spectroscopy energy-momentum conservation rules lead to kinematic restrictions to the experimentally accessible portion of $(Q,\hbar\omega)$ space. In the case of spectroscopy studies of crystalline samples, this limitation can be easily overcome because their translational invariance allows to study the acoustic excitations in high-order Brillouin zones. In the case of topologically disordered systems, the absence of periodicity imposes that the acoustic excitations must be measured at small wave-vector transfer, that is in a region equivalent to the first Brillouin zone in crystals.

For this reason, the present investigation involves room-temperature INS experiments with three different spectrometers operated over complementary dynamic ranges with different energy resolutions. In such a way, access to a wide dynamic range with a resolution adequate to enhance in a clear way the inelastic features under investigation is obtained. Neutron experiments were carried out at the Institute Laue Langevin (Grenoble, France) using both the three-axis IN1 spectrometer and the time-of-flight (TOF) BRIllouin neutron SPectrometer (BRISP) instrument and at the Forschungsneutronenquelle Heinz Maier-Leibnitz, München, Germany (FRM-II) using the TOFTOF spectrometer.[30] In Fig. 1, the dynamic ranges of the three instruments, in the configuration described below in the text, are reported. BRISP supplies the widest dynamic range, but with the worst energy resolution, while TOFTOF has the best resolution, but it can span a narrower energy range. Therefore, further measurements with an intermediate resolution and wider energy range than TOFTOF were performed to bridge the two. High-quality data were obtained using the high flux IN1 instrument. In Table I the measured Q values for each instrument are listed. The INS data treatment included for all spectrometers the standard procedure: subtraction of the empty

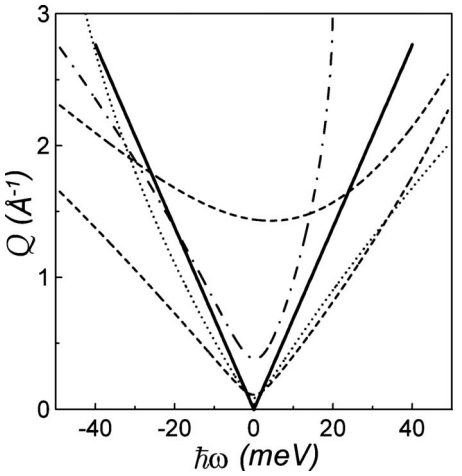

FIG. 1. Dynamic ranges of the three employed instruments: BRISP (dashed lines corresponding to the minimum and maximum angle permitted by the instrument setup), IN1 (dotted line), and TOFTOF (dash-dotted line). Continuous lines represent an extension of the linear acoustic mode dispersion for v-$GeSe_2$ with a sound velocity of 2200 m/s as measured by BLS (Ref. 26).

container and of the multiple scattering signal, correction for the absorption coefficients and for the detector efficiency, normalization to the vanadium standard measurement.

1. IN1

The configuration of IN1 was optimized for operation at small scattering angles (down to 1°) with high-energy resolution using a 1 m diameter vacuum chamber. The crystal analyzer was set to select a fixed final wave vector k_f =4.91 $Å^{-1}$, corresponding to a constant final energy of 50 meV. The resulting elastic resolution was a Gaussian-shaped function with full width at half maximum (FWHM) equal to 1.9 meV, measured using a 2-mm-thick vanadium plate at an intermediate wave vector of 0.45 $Å^{-1}$.

For all the exchanged energies and the measured wave vectors the instrumental resolution has been calculated according to the standard Cooper and Nathans procedure,[31] using the known instrument parameters. The simulated resolution has been checked against the experimental one, giving perfect agreement.

The intensity scattered from the sample was measured at seven different values of wave-vector transfer (see Table I). Because of the small angle configuration, the sample cell was a flat, vacuum tight aluminum cell of dimension of 60 $\times 45 \times 3$ mm^3 with wall thickness of ~0.5 mm. The cell was filled with the $GeSe_2$ powder and the resulting sample transmission was of about 90%.

2. BRISP

The BRISP spectrometer was settled up with the pyrolitic graphite (004) monochromator, which provides a monochromatic neutron beam with a fixed incident wavelength of 0.9885 Å, corresponding to an initial energy of 83.7 meV. The resolution is a Gaussian-shaped function with a FWHM of 2.7 meV. The two-dimensional detector of about 2 m^2 of total active area, installed in a vacuum tank, was placed at a distance of 4 m from the sample. In this configuration, the minimum and maximum scattering angles were about 1° and 13°, respectively, providing the dynamic range reported in Fig. 1. Also in this case, because of the small angle configuration, the sample container was a flat vacuum tight cell with dimension of $50 \times 30 \times 10$ mm^3 with wall thickness of ~0.5 mm, inserted into the vacuum line of the instrument. About 60 gr of $GeSe_2$ powder were filled into the cell, yielding a calculated transmission at the fixed incident wavelength of about 74% in agreement with that experimentally measured during the experiment.

3. TOFTOF

The last set of measurements was performed on the TOF instrument TOFTOF at FRM-II. The incoming wavelength was 2 Å and the resulting resolution was an almost Gaussian-shaped function with a FWHM of 0.3 meV. Given the fact that the sample shape has to match the instrument high scattering angle setup, the powder container was a hollow cylinder of internal and external radius of 9.3 mm and 12.3 mm, respectively, with a wall thickness of ~0.1 mm. This cell was loaded with about 30 g of sample powder in order to have a transmission of more than 90%.

4. Multiple scattering evaluation

Due to the reduced size of the samples and the high transmission, the multiple scattering (MS) contribution to the overall scattering intensity is expected to be generally rather small. However, the total single scattering signal is proportional to $S(Q)$ while the integrated MS is almost angle independent. Therefore in the low-Q region the MS contribution has always to be carefully investigated. With this intent, a Monte Carlo *ad hoc* simulation was performed, according to the approach successfully used in a previous experiment,[32,33] where the correction was rather severe.

Due to the low scattering probability of aluminum metal and the small thickness of the walls, the multiple scattering

TABLE I. List of the Q vector values, which the dynamic structure factor of $GeSe_2$ has been measured at, with the corresponding instruments.

Instrument	Wave-vector transfer Q ($Å^{-1}$)																
IN1	0.30	0.35	0.40	0.45	0.50			0.65		0.75							
BRISP	0.30	0.35	0.40	0.45	0.50	0.55	0.60	0.65	0.70	0.75	0.80	0.85	0.90	0.95	1.00	1.10	1.20
TOFTOF			0.40	0.45	0.50	0.55	0.60	0.65	0.70	0.75	0.80	0.85	0.90	0.95	1.00	1.10	1.20

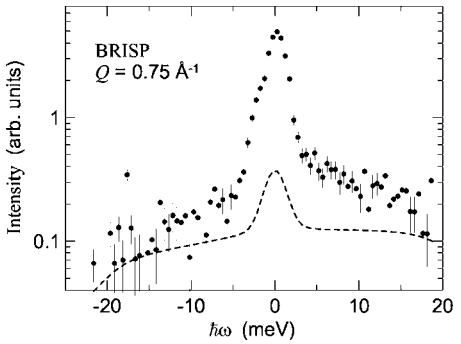

FIG. 2. Example of double scattering contribution (dashed line) compared to the total scattering intensity (full circles) after proper corrections in the case of Q=0.75 Å^{-1} measured with BRISP spectrometer.

events involving the cell were safely neglected and only events inside the sample were considered. Multiple-scattering processes are dominated by the double scattering at high Q in the region close to 90° scattering angle, for which the incoherent approximation is valid and the dynamic structure factor is related to the density of states. The performed simulation assumed a simple model function for the single scattering composed of a narrow Lorentzian quasielastic contribution and steplike function to simulate a Debye density of states

$$S(Q,\omega) = S(Q)\left\{ e^{-2W(Q)} \sqrt{\frac{2\ln 4}{\pi w^2}} e^{-2E^2 \ln 4/w^2} + (1 - e^{-2W(Q)}) \times \left(\frac{\text{arctg}(E+E_D) - \text{arctg}(E-E_D)}{2\pi E_D} \right) \right\}, \quad (1)$$

where $W(Q)$ is the Debye-Waller factor and E_D is the Debye energy for $GeSe_2$ (equal to 20 meV). The simulation took into account the beam shape, the scattering geometry and the density of the powder and provided also the transmission factors as a function of $(Q,\hbar\omega)$. The calculated MS contribution was convoluted with the instrumental resolution function and the resulting intensity was then subtracted from the measured data. An example of the contribution of the multiple scattering to the dynamic structure factor is presented in Fig. 2 for Q=0.75 Å measured with BRISP.

III. EXPERIMENTAL SPECTRA AND DATA ANALYSIS

A selection of spectra obtained with the three instruments at two different wave vectors is shown in Fig. 3, where the instrumental resolution curve and the best fitting function, which will be described in the following, are displayed along with the experimental data. At low momentum transfer, quite defined inelastic peaks can be observed whereas at high Q the inelastic component becomes broad and the peaks are less defined. Thanks to the different energy ranges and resolutions of the three instruments, two defined inelastic peaks can be resolved: one at an almost constant energy of about 2 meV and another fairly broad peak at an energy which increases with Q. On increasing Q, the inelastic component at higher energy becomes broader and broader while the low energy one remains almost constant.

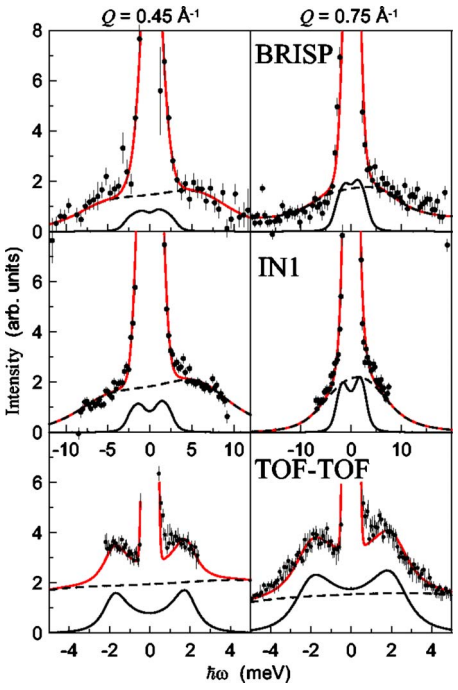

FIG. 3. (Color online) Selection of INS spectra at the indicated wave vectors and instruments as resulting from the complete standard data reduction treatment. The experimental data (black circles) are plotted together with the best-fitting function (continuous red line) and the two inelastic low (continuous black line) and high-frequency (dashed black line) components.

To derive a more quantitative analysis, a convolution of the instrumental resolution and a model function has been fitted to the data. The measured intensity $I(Q,\omega)$ can be expressed in terms of the classical dynamic structure factor $S_{cl}(Q,\omega)$

$$I(Q,\omega) = I_0(Q)R(\omega) \otimes \left\{ S_{cl}(Q,\omega) \frac{\hbar\omega}{k_B T} [n(\omega,T)+1] \right\} \quad (2)$$

convoluted with the instrumental resolution function $R(\omega)$ and multiplied for the Bose-Einstein population factor $[n(\omega,T)+1]$. The overall intensity factor I_0 is a function of the wave vector Q.

The model function can be expressed as the sum of an elastic component and two-inelastic contributions. The elastic peak can be properly described by a delta function $\delta(\omega)$ because the spectra do not show any appreciable broadening around zero energy transfer with respect to the instrument resolution function even in the highest resolution TOFTOF data. Following the prescriptions of the generalized hydrodynamics for harmonic glasses, the simplest description of an acoustic mode is the damped harmonic oscillator (DHO).[34] Therefore, the employed empiric model is

$$S_{cl}(Q,\omega) = A_{el}\delta(\omega) + \frac{A_L(Q)}{\pi}\frac{\Omega_L^2(Q)\Gamma_L(Q)}{[\omega^2-\Omega_L^2(Q)]^2+\omega^2\Gamma_L^2(Q)} + \frac{A_H(Q)}{\pi}\frac{\Omega_H^2(Q)\Gamma_H(Q)}{[\omega^2-\Omega_H^2(Q)]^2+\omega^2\Gamma_H^2(Q)}, \quad (3)$$

where the subscripts refer to the low- (LF-) and high- (HF-) frequency components. The model function of Eq. (3) comprises seven parameters: the intensity of the elastic line $[A_{el}(Q)]$, the intensities of the inelastic components $[A_L(Q)$ and $A_H(Q)]$, their frequencies $[\Omega_L(Q)$ and $\Omega_H(Q)]$ and their damping parameters $[\Gamma_L(Q)$ and $\Gamma_H(Q)]$. The scale factor $I_0(Q)$ depends on the instrument while the intensity parameters $A_{el}(Q)$, $A_L(Q)$, and $A_H(Q)$ are taken equal for the three instruments during the global fitting procedure. We note that the three intensity parameters are not independent one from the other because the energy integral of the total intensity is proportional to the static structure factor $S(Q)$.

Despite the large numbers of parameters, the availability of data with different resolutions and different dynamic ranges allows us to accurately determine the free parameters from an overall fitting procedure. As shown in Table I, the set of the wave-vector transfers can be divided into four groups: *low momentum* common to IN1 and BRISP, *intermediate momentum* common to all the instruments, intermediate momentum common only to BRISP and TOFTOF, *high momentum* common to BRISP and TOFTOF.

The spectra measured with more than one instrument have been fitted using the same set of parameters, apart from the scale factor I_0. In this way each parameter has been accurately determined by a fit as much as possible independent on the starting values and with a reduced number of free parameters. This combined use of the data allows for a safe determination also of the inelastic intensities. In this respect, the role of the high-resolution TOFTOF data, that provide a good determination of the frequency and width of the low energy DHO, should be emphasized. Therefore, the TOFTOF parameters of the low-frequency mode were used for the fit of the BRISP and IN1 spectra. A different situation is settled at low-Q values, for which TOFTOF data are absent. Although IN1 and BRISP have been fitted simultaneously, the parameters of the low-frequency component have to be considered of lower accuracy, both because of the worse resolution and also because the low-energy feature loses progressively its intensity.

IV. VIBRATIONAL DYNAMICS AT TERAHERTZ FREQUENCIES

The peak frequencies, $\Omega_L(Q)$ and $\Omega_H(Q)$ and the corresponding damping parameters $\Gamma_H(Q)$ and $\Gamma_L(Q)$ together with the generalized sound velocities, calculated as $v(Q)=\Omega(Q)/Q$, as a function of wave vector transfer, are displayed in Fig. 4.

The high-frequency mode shows all the typical features of an acoustic mode. The maximum of the dispersion curve occurs around $Q=0.5$ Å^{-1}, i.e., at $Q=Q_P/2$, where Q_P is the position of the FSDP in $S(Q)$, and the dispersion curve goes toward a minimum at Q_P. The low-Q slope of the mode

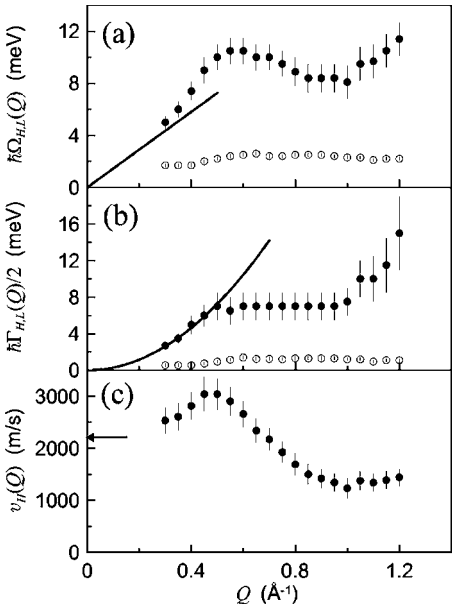

FIG. 4. Open and full circles correspond to the low- and high-frequency components, respectively. Panel (a): dispersion branches for v-$GeSe_2$. The continuous line corresponds to the BLS value (2200 m/s) (Ref. 26). Panel (b): half width of the two modes Γ_L and Γ_H; the line corresponds to a Q^2 law. Panel (c): generalized longitudinal sound velocities derived via $v_H(Q)=\Omega_H(Q)/Q$ for the high-frequency mode. The arrow indicates the 2200 m/s, which represent the continuum limit.

dispersion, determined by fitting the first two points, gives a velocity of 2500 m/s, which is 15% higher than the longitudinal sound velocity (2200 m/s) measured by BLS.[26] A further increase in the longitudinal mode velocity takes place on increasing Q with a maximum values of about 3100 m/s. The HF peak can be associated to the evolution of the longitudinal acoustic mode in the THz frequency range. The positive dispersion of the generalized sound velocity for $Q \sim 0.3$ Å^{-1} is similar to what is found in vitreous silica.[9,10] The positive dispersion is accompanied by the simultaneous observation of the LF excitation with a markedly different behavior. It shows an opticlike character with an almost constant energy of about 2 meV.

The comparison of the present data with experimental results obtained in other systems and with molecular-dynamics simulations[8,11,15,35,36] supports the interpretation of this low-frequency feature as the high-frequency evolution of the transverse acoustic mode, which exists in the continuum limit but should not visible in neutron-scattering experiments. In fact, the inelastic neutron scattering can probe only the longitudinal current correlation function (or density fluctuation) if measured in the first Brillouin Zone. However, it should be noted that the waves sustained by a topologically disordered system can lose their symmetry as the wave vector is increased, so that the *longitudinal* and *transverse* terms lose their precise meaning. Therefore, the visibility of a transverse excitation in neutron spectra can be justified by the mixing phenomenon,[36] which accounts for the fact that at high frequency the transverse dynamics acquire a longitudinal component which is visible in the scattering signal.

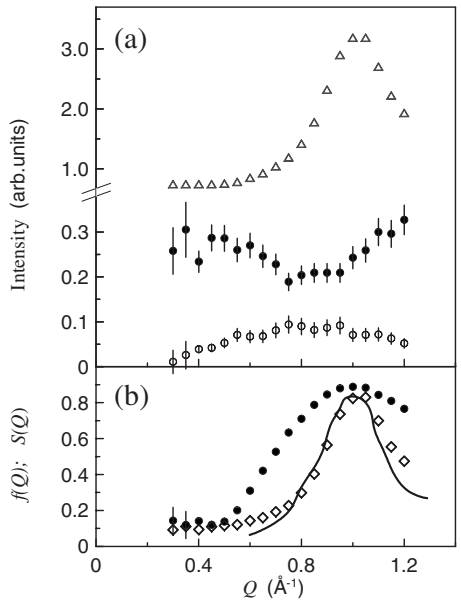

FIG. 5. (a) Integrated elastic intensity (open triangles), integrated inelastic intensity of the low- (open circles), and high- (full circles) frequency mode as a function of Q and (b) nonergodicity factor $f(Q)$ (full circles), calculated as the ratio of the elastic to the total intensity. The total intensity, multiplied by a proper coefficient to fit in the window, is also shown (open diamonds) and compared to the $S(Q)$ (line) from Ref. 22. The nonvisible errors are equal or smaller than the symbol size.

The disorder is also the main responsible for the broadening of the inelastic line. The parameter $\Gamma_H(Q)$ of the high-frequency mode follows the same periodicity of the peak frequency, in agreement with the behavior of other disordered systems, such as ethanol[14] and Se.[13] At low Q, up to about 0.5 Å^{-1}, $\Gamma_H(Q)$ follows the quadratic law depicted in Fig. 4. On increasing Q the H mode becomes overdamped, that is $\Gamma_H(Q)/2 \geq \Omega_H(Q)$, a condition which is reached at about $Q=0.4$ Å^{-1}. The width of the L mode, $\Gamma_L(Q)$, flattens at very small Q.

Additional information can be gained by analyzing the intensity of the various components of the fit. The present data are particularly adequate for this purpose since rather high resolution elastic data are available from the TOFTOF data and wide energy range data are available from BRISP so that the intensity of both inelastic contributions can be safely determined. The integrated intensity of the two inelastic components are reported in Fig. 5(a), where it is seen that there is a trend somewhat connected to the behavior of the static structure factor $S(Q)$. The data reported are limited to those Q values where both BRISP and TOFTOF contribute. Indeed, the TOFTOF data are essential to define the intensity of the low-energy excitation since its intensity can be determined only when it is safely distinguished from the elastic peak. Unfortunately, the available data cannot be efficiently used below 0.4 Å^{-1}, therefore it is difficult to make a conclusive statement about the nature of the low-lying excitation. From the data one can guess a relation between the low-frequency mode and the transverse mode since the intensity of the mode decreases at low Q as it is expected when the mode becomes really transversally polarized. However we cannot rule out the possibility of interpreting the LF mode as an opticlike mode since also this kind of excitation is expected to show a decreasing trend of the intensity as Q is reduced. As to the HF mode, we see a complementary behavior to that of the LF mode and the indication of a flattening of the intensity toward low Q.

Further information can be deduced from the intensity by deriving the nonergodicity parameter $f(Q)=S_{el}(Q)/S(Q)$, where $S_{el}(Q)$ is the integrated intensity of the elastic line of the dynamic structure factor. This quantity is related to the long time plateau of the intermediate scattering function, the Fourier transform of $S(Q,\omega)$. Thanks to the availability of the rather high-resolution data from the TOFTOF experiment it is possible to extract a reliable estimate of $f(Q)$ since the elastic line is accurately determined within a sharp energy window. The data are reported in Fig. 5(b) after correction for the Debye-Waller factor, which accounts for the (almost negligible) vibrational contribution to the elastic line. Since the nonergodicity factor is expected[37] to follow in Q the general trend of the static structure factor, we report in the figure the energy integral of $S(Q,\omega)$ of the present experiments and $S(Q)$ derived from literature diffraction experiments.[20–22] It is worth noting that the intensity data are derived from the whole set of experiments to acquire appropriate information on all the accessible energy windows. We see quite a good agreement between the presently derived $S(Q)$ and that of the diffraction experiment as well as a coherent trend of $f(Q)$, which has a maximum at the position of the first sharp diffraction peak as expected, in agreement with the findings of Ref. 37.

To get more information on the THz dynamics of the $GeSe_2$ glass, the *generalized* vibrational density of states (DOS) has been also determined from the high Q TOFTOF data. The term *generalized* is used to emphasize that is not the true density of states, but its reflection in the scattering, weighted by the cross sections and masses of the atoms in the sample. For a predominantly coherent scattererlike $GeSe_2$, the density of states can be calculated in the framework of the incoherent approximation, which assumes that the interference term in the coherent scattering function averages to zero at relatively high Q and then $S(Q,\omega)$ can be described in terms of an average atom, which scatters only incoherently. For our relatively large Q range, the incoherent approximation is well justified, as demonstrated also for silica and germania.[38] With an iterative self-consistent procedure, one accounts for the entire inelastic scattering including the multiphonon terms and the Debye-Waller factor. The convergence function is the one-phonon density of states. The result showed in Fig. 6 is in good agreement with previous measurements.[20,39,40] The ratio $g(\hbar\omega)/(\hbar\omega)^2$ is also displayed in Fig. 6 as a function of $\hbar\omega$. The plot shows clearly the presence of an excess of DOS (the so called boson peak) with respect to the Debye level, which can be described by means of a logarithmic-normal function.[41,42] The maximum of the boson peak is located at about 1.5 meV. In this regard, it is worth noting that, in the usual data analysis, one performs the fit directly on the experimental quantity, i.e., the $S(Q,\omega)$. The parameter $\Omega(Q)$ of the model function in Eq. (3) represents the position of the maximum of the current $C(Q,\omega)$ spectra while $X_M(Q)$ is the maximum of $S(Q,\omega)$. Straightforward algebra shows that

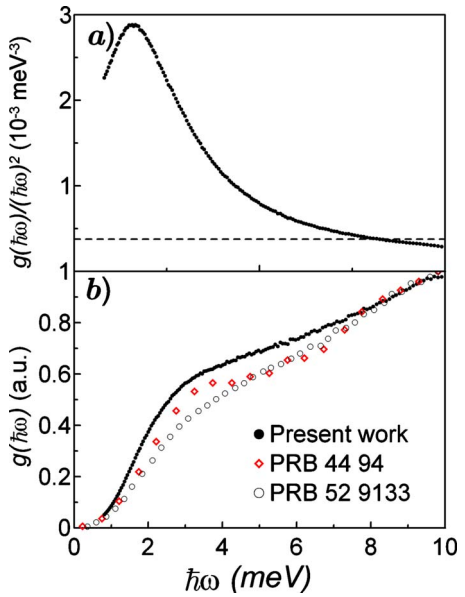

FIG. 6. (Color online) (a) Reduced v-DOS $g(\hbar\omega)/(\hbar\omega)^2$ as a function of energy transfer $\hbar\omega$. The dashed line represents the Debye level. (b) Generalized density of vibrational states measured with TOFTOF spectrometer as a function of energy transfer, normalized to its maximum intensity. The result is in good agreement with previous measurements (diamonds from Ref. 40 and open circles from Ref. 39).

$$\Omega(Q)^2 = X_M^2(Q) + \frac{\Gamma(Q)^2}{2},$$

i.e., the difference between the two maxima is negligible if the width $\Gamma(Q)$ of the peak is small but becomes important at high Q, where $\Gamma(Q)$ is comparable with $\Omega(Q)$. In the latter case, the current peak position is shifted to higher energies when compared to the peaks in $S(Q,\omega)$. The low-frequency excitation energy of Fig. 4 corresponds, therefore, to the energy of the boson peak of Fig. 6. This coincidence suggests that the boson peak could be connected to this LF mode, which, however, we cannot definitively attribute only a transverselike or an opticlike nature to.

With this experimental investigation we get detailed information on the evolution of the modes in a broad Q region, below and above the first sharp diffraction peak. The features of high-frequency-mode dispersion indicates that, even in absence of translational symmetry, the Q value of the FSDP in $S(Q)$ acts as a pseudo reciprocal lattice point for the glass, defining a pseudo-Brillouin zone, thanks to the existence of a medium range order. The entire dispersion curve has been measured only in a few glasses but we can still compare the data of $GeSe_2$ with the results obtained for other strong and fragile systems. A quantitative comparison can be obtained by rescaling the momentum transfer to the position of the FSDP (Q_P) and the frequency with the maximum frequency (Ω_M) of each branch. The results are reported in Fig. 7, where the dispersion curves for glasses with different degrees of fragility, m, are plotted: v-$GeSe_2$ (m=32), v-SiO_2 (m=20), v-GeO_2 (m=24), Se [m=87 (Ref. 43) or m=71 (Ref. 44)] and ethanol (m=52). A universal trend is observed

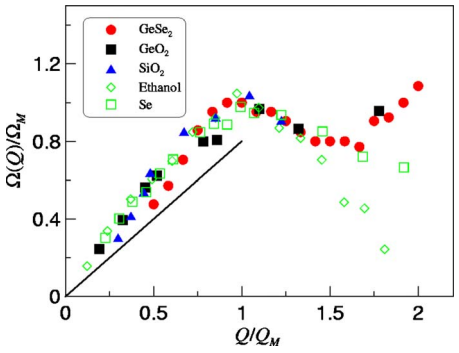

FIG. 7. (Color online) Plot of the dispersion curves of various systems, rescaling the frequencies with the maximum of the branch Ω_M and the wave vector with its position Q_P. Red circles for $GeSe_2$ (this work), black full squares for GeO_2 (Ref. 12), blue triangles for SiO_2 (Refs. 9 and 10) green diamonds for ethanol (Ref. 14), and green open squares for Se (Ref. 13).

when $Q \leq Q_P/2$ while a clear difference between strong glasses and ethanol is present in the region $Q > Q_P/2$. The case of Se is different from this limiting cases: although it has a higher degree of fragility than ethanol it discloses properties similar to strong glasses. In this regard however, it should be noticed that the reported results with IXS show only one point after Q_P.

V. CONCLUSIONS

In this work we presented a detailed study of the high-frequency dynamics in vitreous germanium diselenide using INS. The combined use of three different neutron spectrometers and a properly devised fitting procedure give accurate information on the presence of two rather well-defined modes. The frequency, the width and the intensity of the two modes in a broad Q interval, below and above the first sharp diffraction peak, are derived.

In the investigated Q range, the low-frequency mode is nondispersive and located around the boson peak energy. The high-frequency mode shows the typical features of an acoustic mode: (i) the dispersion relation has a maximum at $Q \approx 0.5$ Å^{-1}, i.e., at $Q \approx Q_P/2$, then it goes toward a shallow minimum at Q_P. (ii) The generalized sound velocity at low Q falls above the hydrodynamic value measured by BLS and reveals a speed up before $Q_P/2$. (iii) The width shows the same pseudoperiodicity of the dispersion curve.

The simultaneous presence of two peaks in the $S(Q,\hbar\omega)$ has been observed in experiments on other amorphous substances, such as water,[45–47] glassy glycerol,[48] silica,[10] and germania.[12] Moreover, also molecular-dynamics simulations confirm the existence of two modes in the dynamic structure factor.[11] The anomalous positive dispersion has been measured, on the contrary, only in vitreous silica.[9]

The pseudoperiodic behavior suggests that the wave vector corresponding to the FSDP acts as a reciprocal lattice point for the glass, defining a pseudo-Brillouin zone. This indicates the existence of a medium-range order in topologically disordered systems. It should be noted that the sinusoidal shape of the dispersion curve should not be considered

as a proof that the high-frequency feature is a unique propagating plane-wave acoustic mode. In fact at these wave vectors the mode damping is comparable to its frequency. The dynamic structure factor thus reflects the spectral distribution of the proper system eigenvectors around the plane-wave component corresponding to the given wave vector Q. However, the periodicity of the dispersion curve demonstrates that an acoustic like component is still present in the spectrum at these high frequencies and that it is affected by the medium range order of the system.

The results obtained on $GeSe_2$ confirm the tendency of other strong glasses, which do not show a sizeable decrease in the frequency of the collective modes when Q exceeds Q_P. A strong difference is seen in comparison to the fragile glass of ethanol, where the dispersion relation above $Q_P/2$ is much more crystal-like, since the frequency approaches a rather low value at the border of the second Brillouin zone.

On one hand, structural differences could be responsible for a different dynamical behavior: glass-forming liquids, such as ethanol, show longer living excitations with a crystal-like acoustic branch and seems to have a higher degree of symmetry, whereas in strong glasses their higher configurational entropy seems to largely affect the vibrational dynamics. This could be connected with the existence of order on different length scales and their appearance in the static structure factor. Strong glasses show a short-range order due to their structural units (tetrahedral structure due to covalent bonding) and their medium-range order is due to strong constraints in the construction of the continuous random network.[49,50] On the contrary, in molecular fragile systems the hydrogen bonds are not sufficient to create a continuous rigid network.[51] The case of selenium is special: there eight-membered puckered rings are present.

On the other hand, another observation should be done in this context: the main difference in the dynamical structure factor of these systems is the presence/absence of the low-energy excitation. In v-$GeSe_2$, v-SiO_2, and v-GeO_2 the clear presence of the nondispersing excitation at small energy has been revealed while in other glass forming materials this second mode is not detected.

However, only limited information, spanning a wide enough Q range in sufficiently spread variety of glasses, are available and this makes it difficult to draw definitive and general conclusions beyond the results of Fig. 7. The observation, embedded in Fig. 7, could lead to new experimental and theoretical interest in the investigation of the frequency dynamics not only in the low frequency regime, which has been the main subject of the last years, but also in the high momentum region.

Finally we underline the relevance of using a set of appropriate instruments in obtaining an accurate determination of the nonergodicity parameter $f(Q)$. The good agreement with the expectation of the mode coupling theory in the observed trend of $f(Q)$ as compared to $S(Q)$ indicates that further experimental effort will be important to determine also the temperature dependence of $f(Q)$ in the region close to the glass transition as it has been done in the case of GeO_2,[37] where only a rough agreement for the temperature dependence has been observed.

ACKNOWLEDGMENTS

We wish to thank the Institut Laue-Langevin (ILL) and the Forschungsneutronenquelle Heinz-Maier-Leibnitz (FRM II) for providing beam time.

*orsingher@science.unitn.it

[1] E. Courtens, M. Foret, B. Hehlen, B. Rufflé, and R. Vacher, J. Phys.: Condens. Matter **15**, S1279 (2003).
[2] B. Rufflé, M. Foret, E. Courtens, R. Vacher, and G. Monaco, Phys. Rev. Lett. **90**, 095502 (2003).
[3] C. Masciovecchio, G. Baldi, S. Caponi, L. Comez, S. Di Fonzo, D. Fioretto, A. Fontana, A. Gessini, S. C. Santucci, F. Sette, G. Viliani, P. Vilmercati, and G. Ruocco, Phys. Rev. Lett. **97**, 035501 (2006).
[4] D. Engberg, A. Wischnewski, U. Buchenau, L. Börjesson, A. J. Dianoux, A. P. Sokolov, and L. M. Torell, Phys. Rev. B **58**, 9087 (1998).
[5] J. L. Feldman, P. B. Allen, and S. R. Bickham, Phys. Rev. B **59**, 3551 (1999).
[6] S. N. Taraskin and S. R. Elliott, Europhys. Lett. **39**, 37 (1997).
[7] T. S. Grigera, V. Martin-Mayor, G. Parisi, and P. Verrocchio, Nature (London) **422**, 289 (2003).
[8] S. N. Taraskin and S. R. Elliott, Philos. Mag. B **77**, 403 (1998).
[9] B. Ruzicka, T. Scopigno, S. Caponi, A. Fontana, O. Pilla, P. Giura, G. Monaco, E. Pontecorvo, G. Ruocco, and F. Sette, Phys. Rev. B **69**, 100201(R) (2004).
[10] G. Baldi, V. M. Giordano, G. Monaco, F. Sette, E. Fabiani, A. Fontana, and G. Ruocco, Phys. Rev. B **77**, 214309 (2008).
[11] O. Pilla, S. Caponi, A. Fontana, J. R. Goncalves, M. Montagna, F. Rossi, G. Viliani, L. Angelani, G. Ruocco, G. Monaco, and F. Sette, J. Phys.: Condens. Matter **16**, 8519 (2004).
[12] L. E. Bove, E. Fabiani, A. Fontana, F. Paoletti, C. Petrillo, O. Pilla, and I. C. V. Bento, Europhys. Lett. **71**, 563 (2005).
[13] T. Scopigno, R. Di Leonardo, G. Ruocco, A. Q. R. Baron, S. Tsutsui, F. Bossard, and S. N. Yannopoulos, Phys. Rev. Lett. **92**, 025503 (2004).
[14] A. Matic, C. Masciovecchio, D. Engberg, G. Monaco, L. Börjesson, S. C. Santucci, and R. Verbeni, Phys. Rev. Lett. **93**, 145502 (2004).
[15] R. Dell'Anna, G. Ruocco, M. Sampoli, and G. Viliani, Phys. Rev. Lett. **80**, 1236 (1998).
[16] C. A. Angell, Science **267**, 1924 (1995).
[17] A. Matic, D. Engberg, C. Masciovecchio, and L. Börjesson, Phys. Rev. Lett. **86**, 3803 (2001).
[18] A. Matic, L. Börjesson, G. Ruocco, C. Masciovecchio, A. Mermet, F. Sette, and R. Verbeni, Europhys. Lett. **54**, 77 (2001).
[19] J. Ruska and H. Thurn, J. Non-Cryst. Solids **22**, 277 (1976).
[20] P. H. Fuoss and A. Fischer-Colbrie, Phys. Rev. B **38**, 1875 (1988).
[21] I. Petri, P. S. Salmon, and H. E. Fischer, Phys. Rev. Lett. **84**, 2413 (2000).

[22] U. Walter, D. L. Price, S. Susman, and K. J. Volin, Phys. Rev. B **37**, 4232 (1988).
[23] W. Zhou, M. Paesler, and D. E. Sayers, Phys. Rev. B **43**, 2315 (1991).
[24] N. Afify, Phys. Rev. B **48**, 16304 (1993).
[25] P. Vashishta, R. K. Kalia, G. A. Antonio, and I. Ebbsjo, Phys. Rev. Lett. **62**, 1651 (1989).
[26] R. J. Nemanich, Phys. Rev. B **16**, 1655 (1977).
[27] A. Feltz, M. Pohle, H. Steil, and G. Herms, J. Non-Cryst. Solids **69**, 271 (1985).
[28] A. J. Dianoux and G. Lander, *Neutron Data Booklet* (Institut Laue Langevin, Grenoble, 2003).
[29] L. Koester, H. Rauch, and E. Seymann, At. Data Nucl. Data Tables **49**, 65 (1991).
[30] T. Unruh, J. Neuhaus, and W. Petry, Nucl. Instrum. Methods Phys. Res. A **580**, 1414 (2007); erratum **585**, 201 (2008).
[31] M. J. Cooper and R. Nathans, Acta Crystallogr. **23**, 357 (1967).
[32] C. Petrillo, F. Sacchetti, B. Dorner, and J.-B. Suck, Phys. Rev. E **62**, 3611 (2000).
[33] C. Petrillo and F. Sacchetti, Acta Cryst. A **46**, 440 (1990); **48**, 508 (1992).
[34] T. Scopigno, G. Ruocco, and F. Sette, Rev. Mod. Phys. **77**, 881 (2005).
[35] S. N. Taraskin, Y. L. Loh, G. Natarajan, and S. R. Elliott, Phys. Rev. Lett. **86**, 1255 (2001).
[36] M. Sampoli, G. Ruocco, and F. Sette, Phys. Rev. Lett. **79**, 1678 (1997).
[37] S. Caponi, M. Zanatta, A. Fontana, L. E. Bove, L. Orsingher, F. Natali, C. Petrillo, and F. Sacchetti, Phys. Rev. B **79**, 172201 (2009).
[38] E. Fabiani, A. Fontana, and U. Buchenau, J. Chem. Phys. **128**, 244507 (2008).
[39] R. L. Cappelletti, M. Cobb, D. A. Drabold, and W. A. Kamitakahara, Phys. Rev. B **52**, 9133 (1995).
[40] W. A. Kamitakahara, R. L. Cappelletti, P. Boolchand, B. Halfpap, F. Gompf, D. A. Neumann, and H. Mutka, Phys. Rev. B **44**, 94 (1991).
[41] V. K. Malinovsky, V. N. Nokikov, P. P. Parshin, A. P. Sokolov, and M. G. Zemlyanov, Europhys. Lett. **11**, 43 (1990).
[42] V. K. Malinovsky, V. N. Nokikov, and A. P. Sokolov, Phys. Lett. A **153**, 63 (1991).
[43] R. Böhmer, K. L. Ngai, C. A. Angell, and D. J. Plazek, J. Chem. Phys. **99**, 4201 (1993).
[44] V. N. Novikov, Y. Ding, and A. P. Sokolov, Phys. Rev. E **71**, 061501 (2005).
[45] F. Sette, G. Ruocco, M. Krisch, C. Masciovecchio, R. Verbeni, and U. Bergmann, Phys. Rev. Lett. **77**, 83 (1996).
[46] G. Monaco, A. Cunsolo, G. Ruocco, and F. Sette, Phys. Rev. E **60**, 5505 (1999).
[47] E. Pontecorvo, M. Krisch, A. Cunsolo, G. Monaco, A. Mermet, R. Verbeni, F. Sette, and G. Ruocco, Phys. Rev. E **71**, 011501 (2005).
[48] T. Scopigno, E. Pontecorvo, R. Di Leonardo, M. Krisch, G. Monaco, G. Ruocco, B. Ruzicka, and F. Sette, Philos. Mag. B **84**, 1453 (2004).
[49] J. C. Phillips, J. Non-Cryst. Solids **34**, 153 (1979).
[50] M. F. Thorpe, J. Non-Cryst. Solids **57**, 355 (1983).
[51] D. Morineau and C. Alba-Simionesco, J. Chem. Phys. **109**, 8494 (1998).